Physical properties of the recently discovered Zr2(Al1−x Bi x)C MAX phases

Hadi, MA, Vovk, RV & Chroneos, A

Original citation & hyperlink:
Hadi, MA, Vovk, RV & Chroneos, A 2016, 'Physical properties of the recently discovered Zr2(Al1−x Bi x)C MAX phases' *Journal of Materials Science: Materials in Electronics*, vol 27, no. 11, pp. 11925-11933
https://dx.doi.org/10.1007/s10854-016-5338-z

DOI 10.1007/s10854-016-5338-z
ISSN 0957-4522
ESSN 1573-482X

Publisher: Springer

The final publication is available at Springer via http://dx.doi.org/10.1007/s10854-016-5338-z

Physical properties of the recently discovered $Zr_2(Al_{1-x}Bi_x)C$ MAX phases

M. A. Hadi,[1] R. V. Vovk[2] and A. Chroneos[3*]

[1]*Department of Physics, University of Rajshahi, Rajshahi 6205, Bangladesh*

[2]*Physics Department, V. Karazin Kharkiv National University, Svobody Sq.4, 61077 Kharkiv, Ukraine*

[3]*Faculty of Engineering, Environment and Computing, Coventry University, Priory Street, Coventry CV1 5FB, United Kingdom*

Abstract

In this study we investigate the structural, electronic and optical properties of the recently synthesized bismuth based $Zr_2(Al_{1-x}Bi_x)C$ MAX phases. It is revealed that the inclusion of Bi in the A site causes an increase of lattice constant *a*, whereas the lattice constant *c* decreases with increasing Bi content *x* up to 0.58. The *c*-values are more influenced than the *a*-values while Al is substituted by Bi, which implies that the *c* value is more dependent on the M-A bonds than the M-X bonds. The calculated band structures imply that the electrical conductivity along the c direction should be small enough compared to that in the ab plane. The low density of states (DOS) around the Fermi level indicate that $Zr_2(Al_{1-x}Bi_x)C$ should be stable in view of electronic structure. The total DOS at the Fermi level increases almost linearly with the increase of the Bi content *x* between 0.25 and 0.75. The Mulliken atomic population calculations indicate that the Zr–C bonds are more covalent in Zr_2BiC than that of Zr_2AlC. The calculated Vickers hardness of Zr_2AlC and Zr_2BiC are calculated to be 5.96 and 1.94 GPa, respectively, implying that Zr_2BiC is relatively soft and easily machinable compared to Zr_2AlC. The calculated optical functions (dielectric constants, refractive index, extinction coefficient, absorption coefficient, loss function, reflectivity, and optical conductivity) show the dependence on the polarization directions.

Keywords: Bismuth based MAX phases; DFT calculations; Electronic properties; Optical functions

PACS numbers: 71.20. Be; 71.15.Mb; 71.20.-b; 78.20-e

[*] Corresponding author email: ab8104@coventry.ac.uk

1. Introduction

The $M_{n+1}AX_n$ phases (n = integer, M = early transition metal; A = group 13-16 element and X = C or N) are materials with the hexagonal $P6_3/mmc$ crystal structure.[1,2] Their important metallic and ceramic properties (high melting temperature, high elastic stiffness, high thermal shock resistance, good machinability, high thermal and electrical conductivity) are borne due to their structure, which consists of the stacking of n "ceramic" layer(s) interleaved by an A "metallic" layer.[3-7] The first member of the family are the M_2AX (or 211 MAX phases), which can be described as a highly symmetric unit cell with atomic layers stacked along the c-direction (refer to Fig. 1).[1,2] The M layers in essence enclose an X layer to form an M_2X slab (with an FCC-type stacking sequence) and the A layers separate these slabs. Finally, the stacking around the A layers has an HPC pattern and the A layers form a mirror plane in the crystal.

Recently, the solid solutions based on MAX phases and ordered quaternary MAX phases have been extensively studied.[8-14] Horlait *et al.*[15] extended the MAX phase family by synthesizing $Zr_2(Al_{1-x}Bi_x)C$ the first bismuth-based MAX phase solid solutions. This study considered the synthesis of this quaternary MAX phase focusing on its relative stability as compared to the end-member ternary compounds.[15] As it was previously discussed the formation of a Zr_2AlC MAX phase would be of interest as a nuclear fuel clad material as Zr has a very high neutron transparency, Al may diffuse out to form an Al_2O_3 layer that could offer high temperature oxidation protection and C does not lead to problematic activation products.[13] The formation of $Zr_2(Al_{1-x}Bi_x)C$ can be an alternative that can lead to further technological applications, as for example act as a precursor for Zr_2C MXenes.[16-19] In the present study, density functional theory (DFT) calculations are employed to calculate the structural, electronic and optical properties of $Zr_2(Al_{1-x}Bi_x)C$ MAX phases.

2. Methodology

The present DFT[20,21] calculations are performed using the plane-wave pseudopotential method as implemented in the CASTEP code.[22] The generalized gradient approximation (GGA) revised by Perdew-Burke-Ernzerhof (PBE) is used to treat the effect of electronic exchange-correlation energy.[23] The interactions between electrons and ion cores are described by the Vanderbilt-type ultrasoft pseudopotentials.[24] The plane-wave energy cutoff is fixed at 600 eV, whereas the k-points mesh[25] of 19×19×4 is used for the Brillouin zone sampling to ensure enough accuracy. The Broyden-Fletcher-Goldfarb-Shanno (BFGS) minimization technique[26] is applied to minimize the total energy and internal forces. The criteria for convergence in geometry optimization are chosen as: the difference in total energy within 5×10^{-6} eV/atom, the ionic Hellmann-Feynman forces within 0.01 eV/Å, maximum stress 0.02 GPa, and the maximum ionic displacement within 5.0×10^{-4} Å. The efficacy of atomistic simulations to describe defect processes has been discussed in previous studies.[27-31]

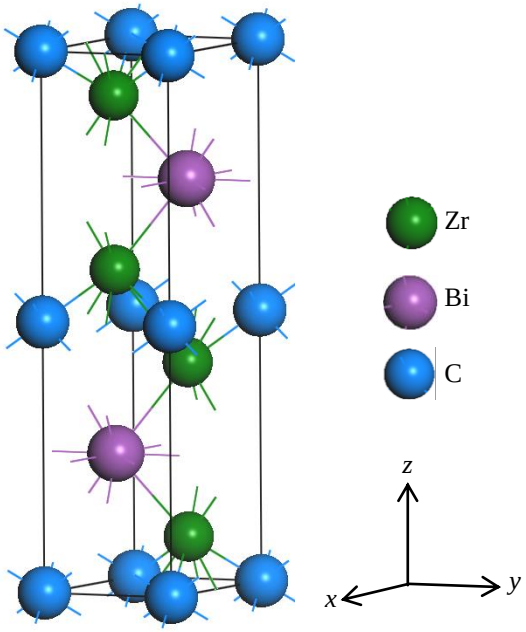

Fig. 1 The unit cell of Zr_2BiC as a structural model of 211 MAX phases

3. Results and discussion

3.1 Structural properties

The calculated equilibrium lattice constants and unit cell volumes for $Zr_2(Al_{1-x}Bi_x)C$ and the two end-members, Zr_2AlC and Zr_2BiC are listed in Table 1 along with the available experimental results.[15,32] The values of the structural properties obtained in the present study are in good agreement with these previous experimental results.[15,32] It is evident from Table 1 that the lattice parameter *a* exhibits the increasing tendency up to $x = 1$ as Bi is incorporated in Zr_2AlC. On the other hand, the lattice constant *c* as well as the hexagonal ratio *c*/*a* shows the decreasing tendencies up to $x = 0.58$. The similar tendencies are observed for the corresponding measured values. When Al is replaced with Bi as in $Zr_2(Al_{1-x}Bi_x)C$, the *c* values are more affected than *a* values, implying that the *c* value is more reliant on the M-A bonds than the M-X bonds. There is a clear change in the lattice constants of the MAX phase solid solution $Zr_2(Al_{1-x}Bi_x)C$ when Bi is incorporated. The optimized unit cell of Zr_2BiC is shown in Fig. 1 as a structural model of 211 MAX phases.

Table 1. The calculated and experimental lattice parameters, hexagonal ratio and unit cell volume of $Zr_2(Al_{1-x}Bi_x)C$ and the end members, Zr_2AlC and Zr_2BiC.

Composition	*a* (Å)	*c* (Å)	*c*/*a*	*V*(Å^3)	Remarks
Zr_2AlC	3.3183	14.6178	4.4052	139.35	This Calc.
	3.3159	14.5756	4.3957	138.79	Expt.[23*]
$Zr_2(Al_{0.75}Bi_{0.25})C$	3.3232	14.2339	4.2832	136.13	This Calc.
$Zr_2(Al_{0.50}Bi_{0.50})C$	3.3559	13.7841	4.1111	134.44	This Calc.
	3.3355	14.512	4.3508	139.84	Expt.[13]
$Zr_2(Al_{0.42}Bi_{0.58})C$	3.3745	13.7216	4.0663	135.32	This Calc.
	3.3445	14.512	4.3391	140.65	Expt.[13]
$Zr_2(Al_{0.25}Bi_{0.75})C$	3.4067	13.8300	4.0596	139.00	This Calc.
Zr_2BiC	3.4390	14.5167	4.2212	148.68	This Calc.

*Average of XRD, SAED and NPD studies.

3.2 Electronic properties

The calculated electronic band structures of $Zr_2(Al_{1-x}Bi_x)C$ solid solutions along the high symmetry directions are shown in Fig. 2. The general features of the electronic band

structures are almost similar for all contents except x = 1. The calculated energy band structures show that the energy band curves pass through the Fermi energy, highlighting the metallic nature of $Zr_2(Al_{1-x}Bi_x)C$ alloys. The energy bands crossing the Fermi level are mainly attributed to the Zr 4d states with some contributions from Zr 5p, Al 3p and/or Bi2 6p states. A significant feature of the band structures near and below the Fermi level is strong anisotropy with less c-axis energy dispersion. This can be observed from the reduced dispersion along the short H–K and M–L directions. Therefore, the electrical conductivity along the c-direction will be lower than that in the ab-plane.

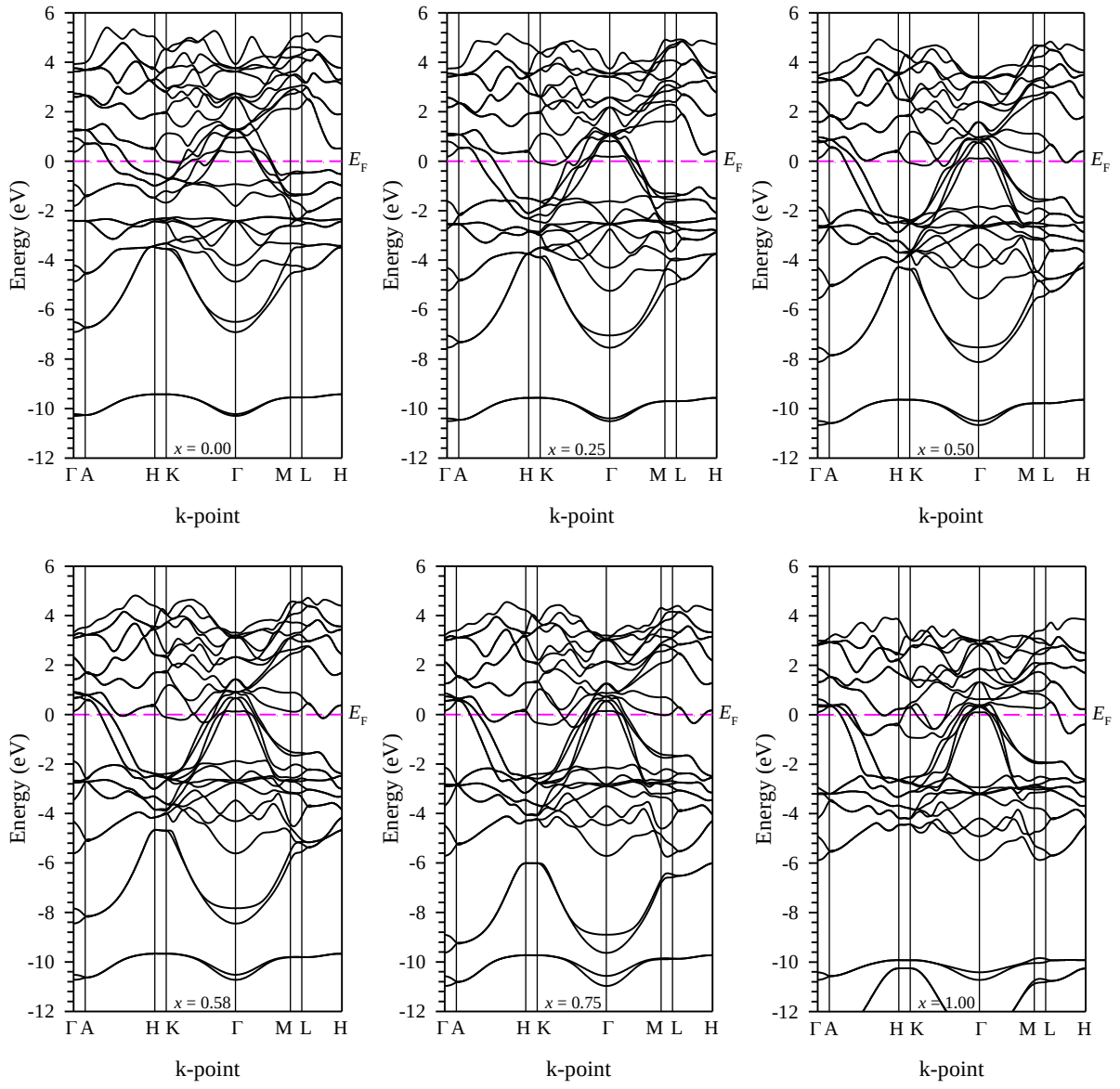

Fig. 2 The calculated band structures of $Zr_2(Al_{1-x}Bi_x)C$ for x = 0.00, 0.25, 0.50, 0.58, 0.75 and 1.00.

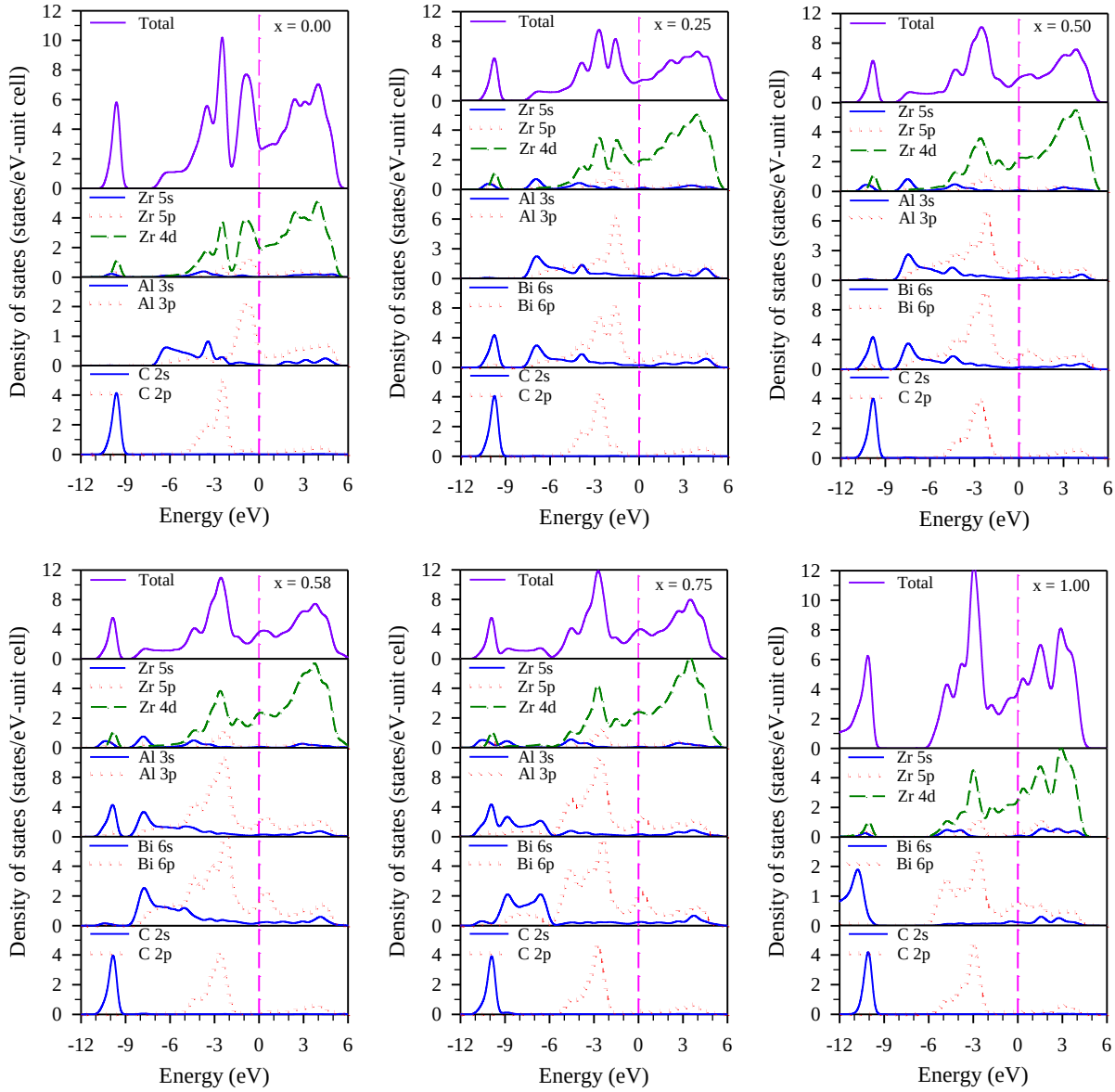

Fig. 3 The calculated density of states of $Zr_2(Al_{1-x}Bi_x)C$ for x = 0.00, 0.25, 0.50, 0.58, 0.75 and 1.00

To investigate the nature of the electronic band structure, we have calculated the total and partial DOS (refer to Fig. 3). In each panel of Fig. 3, the zero energy indicates the Fermi energy that lies in the region of relatively low DOS, indicating to a certain extent that $Zr_2(Al_{1-x}Bi_x)C$ should be stable in perspective of electronic structure according to the free electron model.[33] The atom resolved partial DOS for MAX phases provides more insights on the electronic structure. The occupied part of the DOS can be decomposed in two main regions. The first region lying between –11 and −9 eV (except for Zr_2BiC, x = 1.00 in which –13.4 and −9 eV) consists mainly of C 2s states with some contributions from other electronic

states. The second region from −9 eV to the Fermi energy is mainly derived from Zr 4d states with minor contributions coming from C 2p, Al 3p and/or Bi 6p states. The total values of DOS at the Fermi levels $N(E_F)$ are calculated to be 2.99, 2.61, 3.28, 3.61, 3.92, and 3.82 eV for x = 0.00, 0.25, 0.50, 0.58, 0.75, and 1.00, respectively. It is evident that the $N(E_F)$ with x between 0.25 and 0.75 increases almost linearly as Bi is incorporated in Zr_2AlC. It can also be seen that the double peaks structure in the upper valence band near the E_F for x = 0.00 (Zr_2AlC) reduces significantly for x = 0.25 and completely merges for x ≥ 0.50. As is well known, most of the states at the Fermi energy E_F in MAX phases come from the d orbitals of the transition metal M.[34-40] This is also the case for the $Zr_2(Al_{1-x}Bi_x)C$ MAX phases. Indeed, the DOS contributions from d orbitals of Zr at E_F in $Zr_2(Al_{1-x}Bi_x)C$ are 61–72%. The contributions from C are nearly negligible.

3.3. Mulliken populations and Vickers hardness

The most essential quantities pertaining to atomic bond population calculations are the effective charge and the bond order values between pairs of bonding atoms using minimal basis within the Mulliken scheme[41] as follows, respectively:

$$Q_\alpha^* = \sum_{i,\alpha} \sum_{n\ occ} \sum_{j,\beta} C_{i\alpha}^{*n} C_{j\beta}^{n} S_{i\alpha,j\beta}$$

$$\rho_{\alpha\beta} = \sum_{n\ occ} \sum_{i,j} C_{i\alpha}^{*n} C_{j\beta}^{n} S_{i\alpha,j\beta}$$

where i, j denote the orbital quantum numbers, n is the band index, $C_{i\alpha}^{*n}$ as well as $C_{j\beta}^{n}$ are the eigenvector coefficients of the wave function and $S_{i\alpha,j\beta}$ is the overlap matrix between atoms α and β. The bond hardness for crystal with metallic bonding as proposed by Gou *et al.*[42] is as follows:

$$H_v^\mu = 740\left(P^\mu - P^{\mu'}\right)\left(v_b^\mu\right)^{-5/3}$$

where P^μ is the Mulliken overlap population of the μ-type bond, $P^{\mu'}$ is the metallic population and is evaluated using the unit cell volume V and the number of free electrons in a

cell $n_{free} = \int_{E_P}^{E_F} N(E)dE$ as $P^{\mu'} = n_{free}/V$ and v_b^μ is the volume of a bond of μ-type, which is computed from the bond length d^μ of type μ and the number of bonds N_b^ν of type ν per unit volume by $v_b^\mu = (d^\mu)^3 / \sum_\nu [(d^\mu)^3 N_b^\nu]$. The hardness of a complex multiband compound can be calculated as a geometric average of all bond hardness as follows:[43,44]

$$H_V = [\prod^{\mu} (H_v^\mu)^{n^\mu}]^{1/\Sigma n^\mu}$$

where n^μ is the number of bonds of type μ composing the actual multiband crystal. The effective valence charge and Mulliken atomic population assist to understand the bonding character in solids. The effective valence estimates the difference between the formal ionic charge and Mulliken charge on the anion species in the crystal and verifies the dominance of either covalent or ionic bonding. When the value of effective valence is zero an ideal ionic bond is expected to exist and the values greater than zero indicate an increasing level of covalency. The effective valence listed in Table 2 signifies the prominent covalency in bonding within the two end-members of $Zr_2(Al_{1-x}Bi_x)C$.

Table 2. Population analysis of $Zr_2(Al_{1-x}Bi_x)C$ for x = 0 and 1.

Compounds	Species	Mulliken Atomic populations					Effective valence Charge (e)
		S	p	d	Total	Charge (e)	
Zr_2AlC	C	1.49	3.31	0.00	4.80	–0.80	– –
	Al	1.15	1.92	0.00	3.07	–0.07	3.07
	Zr	2.24	6.64	2.69	11.57	0.43	3.57
Zr_2BiC	C	1.49	3.29	0.00	4.77	–0.77	– –
	Bi	1.66	3.25	0.00	4.91	0.09	3.09
	Zr	2.28	6.58	2.79	11.66	0.34	3.66

Table 3. Calculated Mulliken bond number n^μ, bond length d^μ, and bond overlap population P^μ of μ-type bond of $Zr_2(Al_{1-x}Bi_x)C$ for x = 0 and 1 (with their metallic populations in parenthesis).

Zr_2AlC ($P^{\mu'}$ = 0.0693)				Zr_2BiC ($P^{\mu'}$ = 0.0267)			
Bond	n^μ	d^μ (Å)	P^μ	Bond	n^μ	d^μ (Å)	P^μ
Zr–C	4	2.29376	1.06	Zr–C	4	2.32556	1.11
Zr–Al	4	3.06465	0.73	Zr–Bi	4	3.12997	–0.76
Zr–Zr	2	3.16768	–0.29	Zr–Zr	2	3.13121	–0.07
Al–C	4	4.12520	–0.08	Bi–C	4	4.13762	–0.11

The present method does not allow Mulliken population analysis for disordered crystals. The calculated bond overlap populations for nearest neighbors in the end-members (Zr_2AlC and Zr_2BiC) is presented in Table 3 also assures the above prediction. The overlap population with a value close to zero means that the interaction between the electronic populations of the two atoms is insignificant and a bond with a smallest Mulliken population is extremely weak implying that it can be overlooked in the hardness calculations. A low overlap population is a sign of high degree of ionicity, whereas a high value signifies a high degree of covalency in the chemical bond. The bonding and antibonding states occur due to positive and negative bond overlap populations, respectively. It is observed that the Zr–C bonds are more covalent in Zr_2BiC than that of Zr_2AlC. In Zr_2BiC, the Zr–Bi bonds are observed with negative populations; whereas similar type Zr–Al bonds arise in Zr_2AlC with positive populations. Additionally, a bond forms between two Zr atoms with a small negative populations in Zr_2BiC but the same bond is seen in Zr_2AlC with a high negative populations. The antibonding states in Zr_2AlC are composed mainly from the populations of the bonds Zr–Zr, whereas the populations of Zr–Bi bonds are mainly responsible for these states in Zr_2BiC. The degree of metallicity can be evaluated from $f_m = P^{\mu'}/P^{\mu}$.[42,45] The metallicity of the Zr–C and Zr–Al bonds in Zr_2AlC are calculated to be 0.065 and 0.095, respectively, which indicate the high degree of metallicity in the Zr-Al bonds in comparison to the Zr–C bond. For Zr_2BiC, only the Zr–C bond has metallicity of value 0.024 in the first coordination shell. It can be concluded that the bonding nature in the two end-members of $Zr_2(Al_{1-x}Bi_x)C$ MAX phases can be described as a mixture of covalent and metallic.

Table 4. Calculated Vickers hardness H_v of $Zr_2(Al_{1-x}Bi_x)C$ for x = 0 and 1 with the relevant quantities such as bond volume v_b^{μ} and bond hardness H_v^{μ}.

Compounds	Bond	n^{μ}	d^{μ} (Å)	P^{μ}	$P^{\mu'}$	v_b^{μ} (Å^3)	H_v^{μ} (GPa)	H_v (GPa)
Zr_2AlC	Zr–C	4	2.29376	1.06	0.0693	10.2916	15.0557	5.96
	Zr–Al	4	3.06465	0.73	0.0693	24.5459	2.3583	
Zr_2BiC	Zr–C	4	2.32556	1.11	0.0267	37.1625	1.9370	1.94

Table 4 collects the computed Vickers hardness taking into consideration the positive as well as reasonable populations between nearest neighbors and excluding the populations between next-nearest neighbors in the crystals. The calculated values of the Vickers hardness for Zr_2AlC and Zr_2BiC are 5.96 and 1.94 GPa, respectively. It is obvious that the replacement of Al by Bi reduces the hardness of Zr_2BiC and makes it relatively soft and easily machinable as compared to Zr_2AlC.

3.4. Optical properties

We now reflect on the optical properties for the two end members Zr_2AlC and Zr_2BiC of MAX phase solid solution $Zr_2(Al_{1-x}Bi_x)C$ because CASTEP cannot permit such calculations for disordered crystals. The dielectric function ε(ω) leads to explain the linear response of the system to electromagnetic radiation, which recounts the interaction of photons with electrons. It is well established that the imaginary part $\varepsilon_2(\omega)$ of the dielectric function can be computed via the momentum matrix elements between the occupied and unoccupied wave functions. The real part $\varepsilon_1(\omega)$ of the dielectric function is derived from the Kramer–Kroning relations. The other optical properties can be extracted from the complex dielectric function. The equations employed for calculations of dielectric functions ε(ω), refractive index n(ω), extinction coefficient k(ω), absorption α(ω), energy loss function L(ω), reflectivity R(ω) and optical conductivity σ(ω) are given as follows:

$$\varepsilon_1(\omega) = 1 + \frac{2}{\pi} P \int_0^{\infty} \frac{\omega' \varepsilon_2(\omega') d\omega'}{(\omega'^2 - \omega^2)}$$

$$\varepsilon_2(\omega) = \frac{2e^2\pi}{\Omega\varepsilon_0} \sum_{k,v,c} |\langle \psi_k^c | \boldsymbol{u} \cdot \boldsymbol{r} | \psi_k^v \rangle|^2 \, \delta(E_k^c - E_k^v - E)$$

$$n(\omega) = \frac{1}{\sqrt{2}} \left[\sqrt{\{\varepsilon_1(\omega)\}^2 + \{\varepsilon_2(\omega)\}^2} + \varepsilon_1(\omega) \right]^{1/2}$$

$$k(\omega) = \frac{1}{\sqrt{2}}\left[\sqrt{\{\varepsilon_1(\omega)\}^2 + \{\varepsilon_2(\omega)\}^2} - \varepsilon_1(\omega)\right]^{1/2}$$

$$\alpha(\omega) = \sqrt{2}\omega\left[\sqrt{\{\varepsilon_1(\omega)\}^2 + \{\varepsilon_2(\omega)\}^2} - \varepsilon_1(\omega)\right]^{1/2}$$

$$L(\omega) = \varepsilon_2(\omega)/[\{\varepsilon_1(\omega)\}^2 + \{\varepsilon_2(\omega)\}^2]$$

$$R(\omega) = \left|\frac{\sqrt{\varepsilon(\omega)} - 1}{\sqrt{\varepsilon(\omega)} + 1}\right|^2$$

$$\sigma(\omega) = \frac{\omega\varepsilon_2}{4\pi}$$

All optical calculations are completed with the smearing value as 0.5 eV. A Drude term[46] with unscreened plasma frequency of 3 eV and damping of 0.05 eV is used due to the metallicity of the compounds that is assured in the present electronic structure calculations. The calculated real parts $\varepsilon_1(\omega)$ of dielectric functions of $Zr_2(Al_{1-x}Bi_x)C$ with x = 0 and 1 for two polarization directions [100] and [001] are shown in Fig. 4(left panel). For x = 0 and 1, the main peaks of $\varepsilon_1(\omega)$ arise at around 0.9 eV for both polarization directions. These peaks mainly originate due to transfer of electrons from the top of the valance band to the bottom of the conduction band. A fairly sharp decrease of $\varepsilon_1(\omega)$ spectra is observed in the energy range between 0.9 and 2 eV. Within the energy range 3.1–4.3 eV, the value of $\varepsilon_1(\omega)$ for the both phases turns into negative, and further attains a lowest of $\varepsilon_1(\omega)$ in the range of 5–6.9 eV, and then $\varepsilon_1(\omega)$ increases up to the zero level at higher energies.

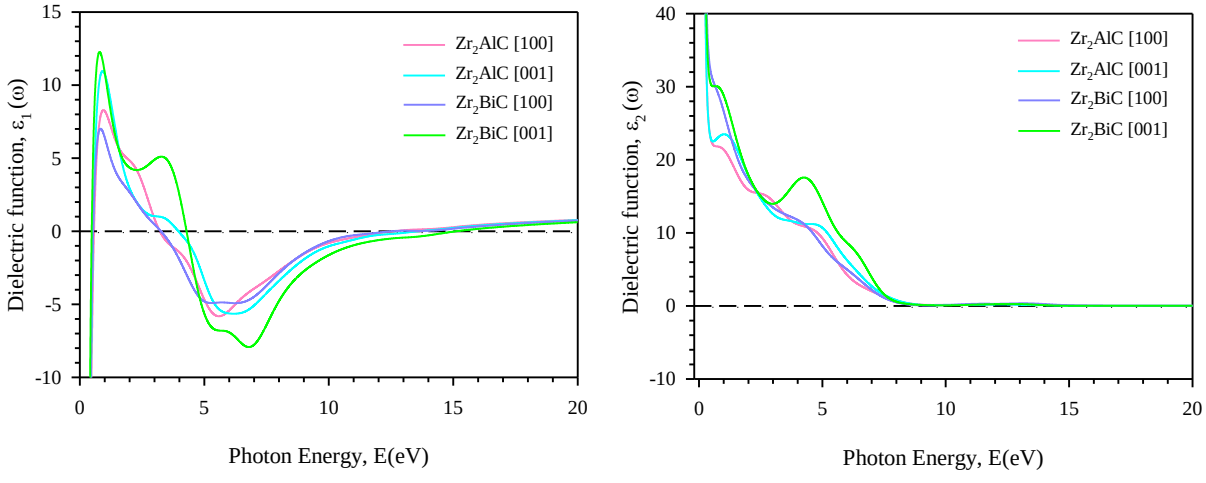

Fig. 4. Real (left) and Imaginary (right) part of dielectric functions of $Zr_2(Al_{1-x}Bi_x)C$ for x = 0 and 1.

The imaginary part $\varepsilon_2(\omega)$ of the dielectric function is the basic issue of the optical properties for materials. The origin of the structures in the imaginary part of the dielectric function can explain the structures in the refractive index. The calculated imaginary parts of the dielectric functions for two end members of $Zr_2(Al_{1-x}Bi_x)C$ are presented in Fig. 4 (right panel). It is seen that the values of $\varepsilon_2(\omega)$ approach zero from above at about 8 eV, which is an additional indication of metallic conductivity of $Zr_2(Al_{1-x}Bi_x)C$. A few numbers of small peaks are observed in the spectra of $\varepsilon_2(\omega)$, which are caused by electron transition. The peak in the low energy region is due to the intra-band transitions, whereas the interband transition is responsible for peaks in the high energy region.

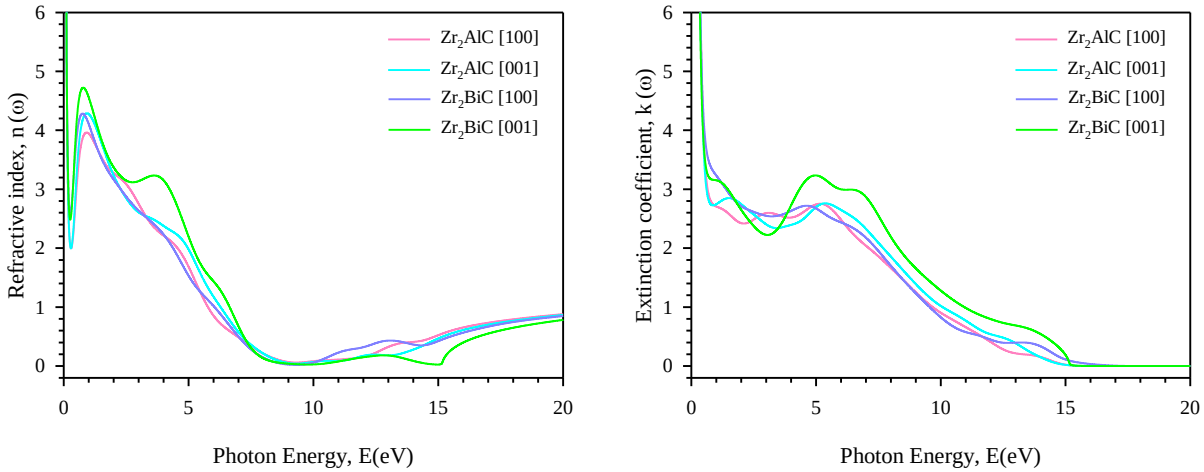

Fig. 5. Refractive index (left) and extinction coefficient (right) of $Zr_2(Al_{1-x}Bi_x)C$ for x = 0 and 1.

The refractive indexes and extinction coefficients of two end members of $Zr_2(Al_{1-x}Bi_x)C$ at different polarization directions are presented in Fig. 5. The knowledge of the refractive index is essential for accurate design of electronic devices. The static refractive index n(0) for incident photon directions [100] and [001] obtained from the dispersion curves of $n(\omega)$ are calculated to be 84.40 and 84.39 for Zr_2AlC and 84.48 and 84.46 for Zr_2BiC, respectively. Refractive indexes decrease drastically in the moderate-infrared region and then increase to their highest peaks at around 0.9 eV. The values of $n(\omega)$ also decrease gradually

with photon energy in the 0.9–9.4 eV region, reaching a minimum value of 0.05 and then increase to a value of 0.87 at about 20 eV. The extinction coefficients k(ω) of Zr_2AlC and Zr_2BiC show the same qualitative features in the whole energy region. The local maxima of the extinction coefficient refer to the zero value of the real part of dielectric function.

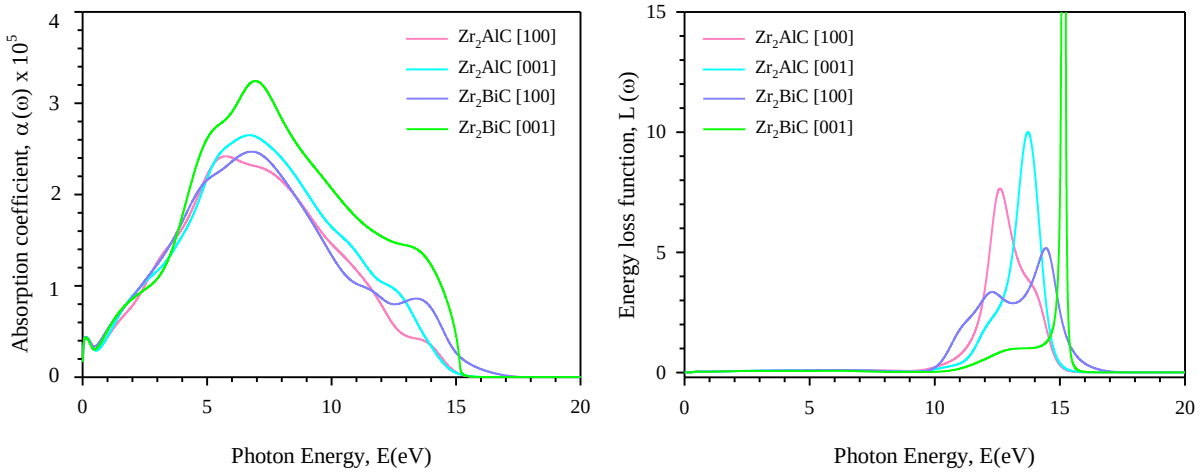

Fig. 6. Absorption coefficient (left) and energy loss function (right) of $Zr_2(Al_{1-x}Bi_x)C$ for x = 0 and 1.

The absorption coefficient is a necessary factor that enlightens the decay of light intensity spreading in unit distance in a medium. According to Fig. 6 (left panel), the absorption spectra begin at zero photon energy, which is the typical feature of metallic compounds. The absorption spectra rise sharply below 5.6 eV and the highest peaks for polarization directions [100] and [001] are found to be located at 5.68 and 6.73 eV for Zr_2AlC and 6.80 and 6.97 eV for Zr_2BiC, respectively. The absorption spectra then decrease drastically with photon energy in the 5.7–15.2 eV region, approaching zero value. The positions and heights of peaks change due to replacement of Al by Bi in Zr_2AlC.

The electron energy-loss function L(ω) is an important factor describing the energy loss of a fast electron traversing in a material. This function can easily be obtained from the imaginary part of the reciprocal of the complex dielectric function. The energy loss spectra in Fig. 6 (right panel) do not exhibit any distinct maxima in the range of about 0–9.7 eV. The cause is that the imaginary part of the dielectric function is still large at these energy values.[47]

In the energy range about 10–17 eV, there is a few number of large peaks in the energy loss spectra. At these high energies, the imaginary part of the dielectric function is small and the amplitude of the energy loss function grows to be large. This function has a main peak associated with the so-called bulk plasma frequency ω_p of the material that appears at $\varepsilon_2 < 1$ and $\varepsilon_1 = 0$.[48] The bulk plasma frequency of Zr_2AlC and Zr_2BiC for incident light directions [100] and [001] are found to be 12.6, 13.7 and 14.5, 15.2 eV, respectively, which correspond to the rapid decrease of reflectivity shown in Fig. 7.

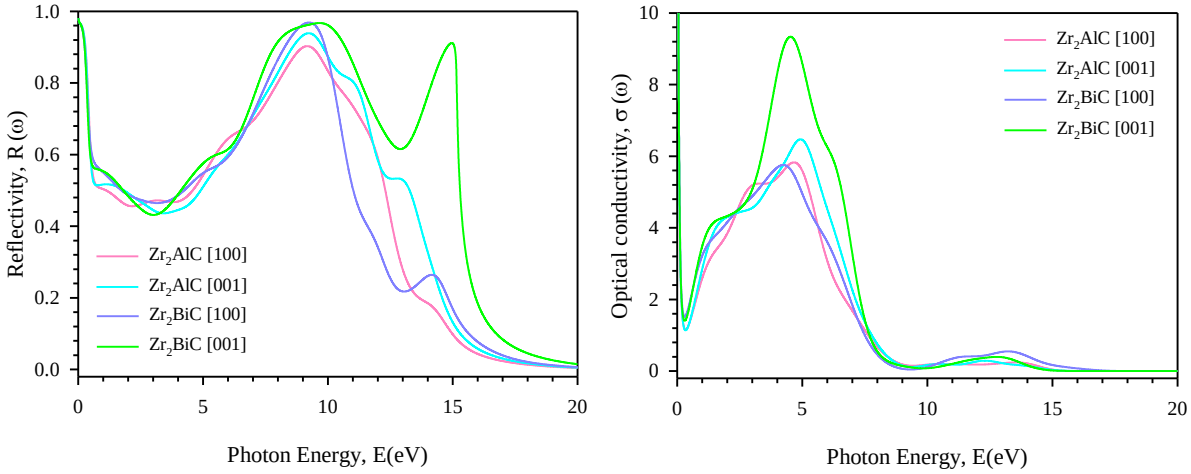

Fig. 7. Reflectivity (left) and optical conductivity (right) of $Zr_2(Al_{1-x}Bi_x)C$ for x = 0 and 1.

The calculated optical reflectivity R(ω) is shown in Fig. 7 (left panel). It is observed that the reflectivity increases drastically in the moderate infrared region as well as in the ultra-violet region to reach their maximum values of 90-97%. In the visible light area (~1.8–3.1 eV) the reflectivity spectra exhibit no considerable change and the amount of reflectivity remains more than 43%, which make the end-members of $Zr_2(Al_{1-x}Bi_x)C$ candidate materials for reducing solar heating.[49] Moreover, due to this nearly constant reflectivity the two MAX compounds should appear as metallic gray.

Optical conductivity may be expected to be a good gauge of photoconductivity that could shed light on the electrical conductivity of the materials. Indeed, it was exemplified in $Nd_2CuO_{4-\delta}$ by means of synchronous measurements of both the optical and photoconductivity. [50]

The real parts of optical conductivities shown in Fig. 7 (right panel) exhibit sharp dip in the energy range 0–0.4 eV and then increase to attain their maximum values in the energy range 4.1–5.0 eV. Within this energy range, the two end-members Zr_2AlC and Zr_2BiC are expected to be highly electrically conductive. It is observed that the peaks' heights of optical conductivities for incident photon direction [001] is larger than that for [100] direction.

4. Conclusions

DFT calculations are employed to predict the lattice parameters, electronic structures and optical functions of the recently discovered Bi-based MAX phase solid solutions $Zr_2(Al_{1-x}Bi_x)C$. The agreement between theoretical and experimental lattice parameters is good. Inclusion of Bi in the A site results in an increase in lattice constant *a*, and a decrease in lattice constant *c* as well as hexagonal ratio *c*/*a* up to $x = 0.58$. The *c* value is more dependent on the M-A bonds than the M-X bonds. Consistently with the end-members, the electronic structures of $Zr_2(Al_{1-x}Bi_x)C$ exhibit metallic-like characters. The electrical conductivity along the c-direction should be smaller than that in the ab plane. The low DOS around the Fermi level is an indication of structural stability of $Zr_2(Al_{1-x}Bi_x)C$. With bismuth content *x* between 0.25 and 0.75 the solid solutions $Zr_2(Al_{1-x}Bi_x)C$ are more conductive than other compositions. According to the results of Mulliken atomic population analysis, the Zr–C bonds are more covalent in Zr_2BiC than that of Zr_2AlC. The Vickers hardness of Zr_2AlC (5.96 GPa) and Zr_2BiC (1.94 GPa) show that the latter is relatively softer and easily machinable. The optical properties (dielectric functions, refractive index, extinction coefficient, absorption coefficient, energy loss function, reflectivity and optical conductivity) are calculated to be polarization dependent. Moreover, the reflectivity spectra in the visible light region constitute Zr_2AlC and Zr_2BiC potential candidate materials for coatings to reduce solar heating.

Acknowledgments

A.C. is grateful for funding from the Lloyd's Register Foundation, a charitable foundation helping to protect life and property by supporting engineering-related education, public engagement and the application of research.

References

1 H. Nowotny, *Prog. Solid State Chem.*, 1970, **2**, 27.
2 M. W. Barsoum, and M. Radovic, *Ann. Rev. Mater. Res.*, 2011, **41**, 195.
3 M. W. Barsoum, and T. El-Raghy, *J. Am. Ceram. Soc.*, 1996, **79**, 1953.
4 M. W. Barsoum, D. Brodkin, and T. El-Raghy, *Scr. Met. Mater*., 1997, **36**, 535.
5 M. W. Barsoum, B. G. Yaroschuck, and S. Tyagi, *Scr. Met. Mater*., 1997, **37**, 1583.
6 T. Lapauw, J. Halim, J. Lu, T. Cabioc'h, L. Hultman, M. W. Barsoum, K. Lambrinou, and J. Vleugels, *J. Eur. Ceram. Soc.*, 2016, **36**, 943.
7 T. Lapauw, K. Vanmeensel, K. Lambrinou, and J. Vleugels, *Scr. Mater.*, 2016, **111**, 98.
8 D. Horlait, S. Grasso, A. Chroneos, and W. E. Lee, *Mater. Res. Lett*., (2016) DOI: 10.1080/21663831.2016.1143053
9 B. Anasori, M. Dahlqvist, J. Halim, E. J. Moon, J. Lu, B. C. Hosler, E. N. Caspi, S. J. May, L. Hultman, P. Eklund, J. Rosén, M. W. Barsoum, *J. Appl. Phys*. 2015, **118**, 094304.
10 B. Anasori, J. Halim, J. Lu, C. A. Voigt, L. Hultman, M. W. Barsoum, *Scr. Mater*., 2015, **101**, 5.
11 E. N. Caspi, P. Chartier, F. Porcher, F. Damay, T. Cabioc'h, *Mater. Res. Lett*., 2015, **3**, 100.
12 M. Naguib, G. W. Bentzel, J. Shah, J. Halim, E. N. Caspi, J. Lu, L. Hultman, M. W. Barsoum, *Mater. Res. Lett*., 2014, **2**, 240.
13 Z. Liu, E. Wu, J. Wang, Y. Qian, H. Xiang, X. Li, Q. Jin, G. Sun, X. Chen, J. Wang, M. Li, *Acta Mater*., 2014, **73**, 186.
14 Y. Zhou, F. Meng, J. Zhang, *J. Amer. Ceram. Soc*., 2008, **91**, 1357.
15 D. Horlait, S. C. Middleburgh, A. Chroneos, and W. E. Lee, *Sci. Rep.*, 2016, **5**, 18829.
16 S. J. Zhao, W. Kang, and J. M. Xue, *Appl. Phys. Lett.*, 2014, **104**, 133106.
17 J. J. Zhu, A. Chroneos, and U. Schwingenschlögl, *Phys. Stat. Sol. RRL*, 2015, **9**, 726.
18 D. Cakir, C. Sevik, O. Gulseren, and F. M. Peeters, *J. Mater. Chem. A*, 2016, **4**, 6029.
19 M. Khazaei, A. Ranjbar, M. Ghorbani-Asl, M. Arai, T. Sasaki, Y. Y. Liang, and S. Yunoki, *Phys. Rev. B*, 2016, **93**, 205125.
20 P. Hohenberg, and W. Kohn, *Phys. Rev.*, 1964, **136**, B864.
21 W. Kohn, and L. J. Sham, *Phys. Rev*., 1965, **140,** A1133.
22 S. J. Clark, M. D. Segall, C. J. Pickard, P. J. Hasnip, M. I. J. Probert, K. Refson, and M. C. Payne, *Zeitschrift für Kristallographie*, 2005, **220,** 567.
23 J. P. Perdew, K. Burke, and M. Ernzerhof, *Phys. Rev. Lett*., 1996, **77**, 3865.
24 Vanderbilt, *Phys. Rev. B*, 1990, **41**, 7892.
25 H. J. Monkhorst and J. D. Pack, *Phys. Rev. B*, 1976, **13**, 5188.
26 T. H. Fischer and J. Almlof, *J. Phys. Chem*., 1992, **96**, 9768.
27 R. W. Grimes, G. Busker, M. A. McCoy, A. Chroneos, J. A. Kilner, and S. P. Chen, *Ber. Bunsen-Ges.*, 1997, **101**, 1204.
28 A. Chroneos, C. Jiang, R. W. Grimes, U. Schwingenschlögl, and H. Bracht, *Appl. Phys. Lett.*, 2009, **95**, 112101.

29 D. Rupasov, A. Chroneos, D. Parfitt, J. A. Kilner, R. W. Grimes, S. Y. Istomin, and E. V. Antipov, *Phys. Rev. B*, 2009, **79**, 172102.
30 S. T. Murphy, A. Chroneos, C. Jiang, U. Schwingenschlögl, and R. W. Grimes, *Phys. Rev. B*, 2010, **82**, 073201.
31 A. Chroneos, C. A. Londos, and E. N. Sgourou, *J. Appl. Phys.*, 2011, **110**, 093507.
32 T. Lapauw, K. Lambrinou, T. Cabioc'h, J. Halim, J. Lu, A. Pesach, O. Rivin, O. Ozeri, E. N. Caspi, L. Hultman, P. Eklund, J. Rosén, M. W. Barsoum, and J. Vleugels, *J. Eur. Ceram. Soc.*, 2016, **36**, 1847.
33 S. Nagel and J. Tauc, *Phys. Rev. Lett.*, 1975, **35,** 380.
34 M. T. Nasir, A. K. M. A. Islam, *Comp. Mater. Sci*., 2012, **65**, 365.
35 Y. Mo, P. Rulis, and W. Y. Ching, *Phys. Rev. B*, 2012, **86**, 165122.
36 M. Roknuzzaman, A. K. M. A. Islam, *ISRN Condens. Matter Phys*., 2013, **2013**, 646042.
37 M. A. Hadi, M. Roknuzzaman, F. Parvin, S. H. Naqib, A. K. M. A. Islam, M. Aftabuzzaman, *J. Sci. Res*., 2014, **6**, 11.
38 M. T. Nasir, M. A. Hadi, S. H. Naqib, F. Parvin, A. K. M. A. Islam, M. Roknuzzaman, M.S. Ali, *Int. J. Mod. Phys. B*, 2014, **28**, 1550022.
39 M. Roknuzzaman, M. A. Hadi, M. J. Abden, M. T. Nasir, A. K. M. A. Islam, M. S. Ali, K. Ostrikov, S. H. Naqib, *Comp. Mater. Sci*., 2016, **113**, 148.
40 M. A. Hadi, *Comp. Mater. Sci*., 2016, **117**, 422.
41 R. S. Mulliken, *J. Chem. Phys.*, 1955, **23**, 1833.
42 H. Gou, L. Hou, J. Zhang, and F. Gao, *Appl. Phys. Lett*., 2008, **92**, 241901.
43 A. Szymański and J. M. Szymański, Hardness Estimation of Minerals Rocks and Ceramic Materials, 6th edition, Elsevier, Amsterdam, 1989.
44 V. M. Glazov and V. N. Vigdorovid, Hardness of Metals, Izd. Metellurgiya, Moskva, 1989.
45 M. A. Hadi, M. S. Ali, S. H. Naqib, and A. K. M. A. Islam, *Int. J. Comp. Mater. Sci. Eng.*, 2013, **2**, 1350007.
46 R. Saniz, L. H. Ye, T. Shishidou, and A. Freeman, *J Phys. Rev. B*, 2006, **74**, 014209.
47 J. P. Watt, L. Peselnick, *J. Appl. Phys*., 1980, **51**, 1525.
48 J. S. de Almeida and R. Ahuja, *Phys. Rev. B*, 2006, **73**, 165102.
49 S. Li, R. Ahuja, M. W. Barsoum, P. Jena and B. Johansson, *Appl. Phys. Lett*., 2008, **92**, 221907.
50 G. Yu, C. H. Lee, A. J. Heeger, and S. W. Cheong, *Physica C*, 1992, **203**, 419.